Inorganic Chemistry
Article

Inorg. Chem. **2009**, *48*, 5861–5873 **5861**
DOI: 10.1021/ic900128t

Investigation of Flexible Organic Ligands in the Molybdate System: Delicate Influence of a Peripheral Cluster Environment on the Isopolymolybdate Frameworks

Bao-xia Dong and Qiang Xu*

National Institute of Advanced Industrial Science and Technology (AIST), Ikeda, Osaka 563-8577, Japan

Received January 21, 2009

By introducing the flexible 1,4-bis(1,2,4-triazol-1-ylmethyl)benzene (L^1) and 1,4-bis(imidazole-1-ylmethyl)benzene (L^2) ligands into the molybdate system under hydrothermal conditions, 12 novel isopolymolybdate frameworks were obtained: $[CuL^1(H_2O)][Mo_3O_{10}]$ (**1**), $[ML^1(H_2O)_2][Mo_3O_{10}]$ [M = Cu (**2**), Zn (**3**), and Co (**4**)], $[Cu_2(L^1)_4][\theta\text{-}Mo_8O_{26}]$ (**5**), $[Cu_4(L^1)_4][\beta\text{-}Mo_8O_{26}]_{0.5}[\gamma\text{-}Mo_8O_{26}]_{0.5}\cdot H_2O$ (**6**), $[Ag_4(L^1)_2][\beta\text{-}Mo_8O_{26}]$ (**7**), $[M_2(L^1)_3(H_2O)_4][\beta\text{-}Mo_8O_{26}]\cdot 2H_2O$ [M = Zn (**8**), Co (**9**), and Ni (**10**)], and $[M_4(L^2)_4][\delta\text{-}Mo_8O_{26}]$ [M = Cu (**11**) and Ag (**12**)]. Compound **1** and isostructural compounds **2**−**4** exhibit similar three-dimensional (3D) pillar-layered structures. Compound **5** shows a novel pillar-layered framework constructed from two sorts of $[CuL^1]_n$ left- and right-handed helical chains and the θ-$[Mo_8O_{26}]^{4-}$ polyoxoanion. Compound **6** contains two sorts of isomers of β-$[Mo_8O_{26}]^{4-}$ and γ-$[Mo_8O_{26}]^{4-}$ coexisting in one structure, which induce the formation of two sorts of ladderlike building blocks and finally the polythread structure. The cationic and anionic fragments in compound **7**, the dinuclear molecular loop of $[Ag_2(L^1)_2]^{2+}$ and β-$[Mo_8O_{26}]^{4-}$, are both linked up by single Ag ions, forming two kinds of infinite chains of $[Ag_3(L^1)_2]_n^{3n+}$ and $[Ag\text{-}\beta\text{-}Mo_8O_{26}]_n^{3n-}$, respectively. Compounds **8**−**10** are isostructural and exhibit the parallel two-fold (2D→2D) interpenetrated networks based on the β-$[Mo_8O_{26}]^{4-}$ cluster. Isostructural compounds **11** and **12** have 3D polythread penetrated frameworks based on the δ-$[Mo_8O_{26}]^{4-}$ polyoxoanion. The luminescent properties of the ligands and complexes **3**, **6**−**8**, and **11**−**12** are investigated in the solid state.

Introduction

Polyoxometalates (POMs) that represent an outstanding class of molecules with unrivaled versatility and attractive guest absorption properties[1] have attracted long-lasting interest in photochemistry,[2] electrochemistry,[3] magnetism,[4] catalysis,[5] biochemistry, and pharmaceutical chemistry.[6] In this field, a powerful synthetic approach for the design of high-dimensional hybrid materials which possess unique structures and properties uses the coordination ability of the polyoxoanion to combine with different transition-metal coordination polymers. Through the introduction of the transition metal complexes (TMCs), these polyoxoanions, acting as unusual inorganic ligands, can multiply bind several of the TMCs through the coordination of their terminal or bridge oxygen atoms.[7−9] As is well-known, POMs are a kind

*To whom correspondence should be addressed. Tel.: (+81) 72-751-9652. Fax: (+81) 72-751-7942. E-mail: q.xu@aist.go.jp.

(1) (a) Jiang, C. J.; Lesbani, A.; Kawamoto, R.; Uchida, S.; Mizuno, N. *J. Am. Chem. Soc*. **2006**, *128*, 14240. (b) Uchida, S.; Hashimoto, M.; Mizuno, N. *Angew. Chem., Int. Ed. Engl*. **2002**, *41*, 2814. (c) Kawamoto, R.; Uchida, S.; Mizuno, N. *J. Am. Chem. Soc*. **2005**, *127*, 10560. (d) Ishii, Y.; Takenaka, Y.; Konishi, K. *Angew. Chem., Int. Ed. Engl*. **2004**, *43*, 2702.

(2) (a) Kögerler, P.; Cronin, L. *Angew. Chem., Int. Ed. Engl*. **2005**, *44*, 844. (b) Yamase, T. *J. Chem. Soc., Dalton Trans*. **1985**, 2585.

(3) Coronado, E.; Galán-Mascarós, J. R.; Giménez-Saiz, C.; Gómez-García, C. J.; Martínez-Ferrero, E.; Almeida, M.; Lopes, E. B. *Adv. Mater*. **2004**, *16*, 324.

(4) (a) Pope, M. T.; Müller, A. *Angew. Chem., Int. Ed. Engl*. **1991**, *30*, 34. (b) Müller, A. *Nature (London)* **1991**, *352*, 115. (c) Gouzerh, P.; Villaneau, R.; Proust, R.; Delmont, A. *Chem.−Eur. J*. **2000**, *6*, 1184. (d) Artero, V.; Proust, A.; Herson, P.; Gouzerh, P. *Chem.−Eur. J*. **2001**, *7*, 3901. (e) Liu, T.; Diemann, E.; Li, H.; Dress, A.; Müller, A. *Nature (London)* **2003**, *426*, 59. (f) Salignac, B.; Riedel, S.; Dolbecq, A.; Secheresse, F.; Cadot, E. *J. Am. Chem. Soc*. **2000**, *122*, 10381. (g) Coronado, E.; Gómez-García, C. J. *Chem. Rev*. **1998**, *98*, 273. (h) Coronado, E.; Giménez-Saiz, C.; Gómez-García, C. J. *Coord. Chem. Rev*. **2005**, *249*, 1776.

(5) (a) Müller, A.; Pope, M. T.; Peters, F.; Gatteschi, D. *Chem. Rev*. **1998**, *98*, 239. (b) Artero, V.; Proust, A.; Herson, P.; Villain, F.; Moulin, C.; Gouzerh, P. *J. Am. Chem. Soc*. **2003**, *125*, 11156.

(6) (a) Rhule, J. T.; Hill, C. L.; Judd, D. A. *Chem. Rev*. **1998**, *98*, 327. (b) Wang, X.; Liu, J.; Pope, M. *Dalton Trans*. **2003**, 957.

(7) (a) Liu, C. M.; Zhang, D. Q.; Xiong, M.; Zhu, D. B. *Chem. Commun*. **2002**, 1416. (b) Yuan, M.; Li, Y. G.; Wang, E. B.; Tian, C. G.; Wang, L.; Hu, C. W.; Hu, N. H.; Jia, H. Q. *Inorg. Chem*. **2003**, *42*, 3670. (c) Lin, B. Z.; Liu, S. X. *Chem. Commun*. **2002**, 2126. (d) Zhang, L. J.; Zhao, X. L.; Xu, J. Q.; Wang, T. G. *Dalton Trans*. **2002**, 3275.

(8) (a) Cui, X. B.; Xu, J. Q.; Li, Y.; Sun, Y. H.; Yang, G. Y. *Eur. J. Inorg. Chem*. **2004**, 1051. (b) Zheng, S. T.; Chen, Y. M.; Zhang, J.; Xu, J. Q.; Yang, G. Y. *Eur. J. Inorg. Chem*. **2006**, 397. (c) Liu, C. M.; Zhang, D. Q.; Zhu, D. B. *Cryst. Growth Des*. **2006**, *6*, 524.

(9) (a) Ren, Y. P.; Kong, X. J.; Long, L. S.; Huang, R. B.; Zheng, L. S. *Cryst. Grouth Des*. **2006**, *6*, 572. (b) An, H. Y.; Wang, E. B.; Xiao, D. R.; Li, Y. G.; Su, Z. M.; Xu, L. *Angew. Chem., Int. Ed*. **2006**, *45*, 904. (c) Luan, G. Y.; Li, Y. G.; Wang, S. T.; Wang, E. B.; Han, Z. B.; Hu, C. W.; Hu, N. H.; Jia, H. Q. *Dalton Trans*. **2003**, 233. (d) Lu, Y.; Xu, Y.; Wang, E. B.; Lü, J.; Hu, C. W.; Xu, L. *Cryst. Growth Des*. **2005**, *5*, 257. (e) Han, Z. G.; Zhao, Y. L.; Peng, J.; Ma, H. Y.; Liu, Q.; Wang, E. B.; Hu, N. H.; Jia, H. Q. *Eur. J. Inorg. Chem*. **2005**, 264.

Published on Web 05/21/2009

of competent structure-tunable building block because they exhibit a wide variety of robust structural motifs of different sizes and topologies, ranging from closed cages and spherical shells to basket-, bowl-, barrel-, and belt-shaped structures.[10] A common example is the octamolybdate anion $[Mo_8O_{26}]^{4-}$, for which eight isomeric forms, α through θ, have been reported.[11] Therefore, the use of POMs as inorganic building blocks brews an appealing route to the design of novel structural motifs with improved properties.

Recently, there has been increasing interest in applications of flexible ligands as linkers together with specific polyoxoanion building blocks to build high-dimensional polymeric arrays.[12] The flexible bridging ligands are regarded as a class of excellent synthons for the construction of functional porous coordination polymer materials due to their flexibility and conformation freedom.[13,14] It is especially attractive that they are inclined to conform to the coordination environment of metal ions and, further, the polyoxoanion templates when they are introduced into the POM system. This character is embodied in our work that used the flexible 1,1′-(1,4-butanediyl)bis(imidazole) (bbi) ligand to assemble big clusters of spherical $[As_8V_{14}O_{42}]^{4-}$ and ellipsoidal $[V_{16}O_{38}Cl]^{6-}$ polyoxovanadate anions and Keggin-type $[PW_{12}O_{40}]^{3-}$ anions together with metal ions.[15] Systematic polyoxoanion-templated architectures have been obtained in such attempts. The flexible bbi has also been employed by other researchers for the construction of supramolecular isomers based on the octamolybdate anion $[Mo_8O_{26}]^{4-}$.[16] Furthermore, by tuning the length of flexible bis(triazole) ligands, Wells−Dawson-based hybrid frameworks have been synthesized with the highest connectivity for such types of polyoxoanion to date.[17] Most recently, an antifungal medicine, [2-(2,4-difluorophenyl)-1,3-di(1H-1,2,4-triazol-1-yl)propan-2-ol], which is also a flexible 1,2,4-triazole derivative, has been chosen to act as the bridging ligand in the β-$[Mo_8O_{26}]^{4-}$ system.[18] This work illustrates that different coordination behaviors of metal ions exert a strong influence on the coordination mode of the β-$[Mo_8O_{26}]^{4-}$ anion and, further, the framework in each compound. All of these examples made us more convinced that flexible ligands would have a profound influence on the POM system and would be more popular in the near future.

Scheme 1

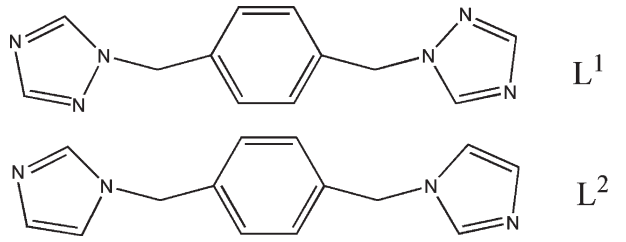

Hereafter, we put an emphasis on flexible ligands in the isopolymolybdate system. As mentioned above, octamolybdate is a common building block which has been extensively explored as an analogue to oxide surfaces and as potential catalysts.[19] In the course of designing new organic−inorganic hybrid materials with interesting properties, we introduce two similar flexible N-heterocyclic ligands based on bis-(1,2,4-triazole) and bis-imidazole molecules, respectively, 1,4-bis(1,2,4-triazol-1-ylmethyl)benzene (L^1) and 1,4-bis(imidazole-1-ylmethyl)benzene (L^2), into the isopolymolybdate system (Scheme 1). In light of previous studies, we are convinced that the coordination numbers and geometries of the transition metal ions play an important role in the assembly process. The present study focuses on two questions: (i) Do different transition metal ions have any influence on the isomeric forms of the $[Mo_8O_{26}]^{4-}$ cluster when the same ligand is used? (ii) Do flexible ligands with minor differences have any delicate influence on the isopolymolybdate frameworks as well as the isomeric forms of the $[Mo_8O_{26}]^{4-}$ cluster when the same metal ion is used? This paper concentrates principally on the self-assembly of transition metal ions Cu^{2+}, Cu^{+}, Ag^{+}, Zn^{2+}, Co^{2+}, and Ni^{2+} toward isopolymolybdate bridging ligands L^1 and L^2 under hydrothermal conditions. A series of novel compounds built upon four types of $[Mo_8O_{26}]^{4-}$ isomers and one kind of $[Mo_3O_{10}]^{2-}$ polyoxoanion were synthesized, namely, $[CuL^1(H_2O)][Mo_3O_{10}]$ (**1**), $[ML^1(H_2O)_2][Mo_3O_{10}]$ [M = Cu (**2**), Zn (**3**), and Co (**4**)], $[Cu_2(L^1)_4][Mo_8O_{26}]$ (**5**), $[Cu_4(L^1)_4][Mo_8O_{26}]\cdot H_2O$ (**6**), $[Ag_4(L^1)_2][Mo_8O_{26}]$ (**7**), $[M_2(L^1)_3(H_2O)_4][Mo_8O_{26}]\cdot 2H_2O$ [M = Zn (**8**), Co (**9**), and Ni (**10**)], and $[M_4(L^2)_4][Mo_8O_{26}]$ [M = Cu (**11**) and Ag (**12**)] (Scheme 2). In this work, we also report the luminescent properties of the ligands and complexes **3**, **6**−**8**, and **11**−**12** in the solid state.

Experimental Section

Materials and General Method. All chemicals purchased were of reagent grade and were used as received. The ligands L^1 and L^2 were prepared according to the reported procedure.[20] FTIR spectra (KBr pellets) were recorded in the range of 2000−450 cm^{-1} on a BRUKER IFS 66v/S Fourier-transform infrared

(10) (a) Klemperer, W. G.; Marquart, T. A.; Yagi, O. M. *Angew. Chem., Int. Ed.* **1992**, *31*, 49. (b) Day, V. W.; Klemperer, W. G.; Yagi, O. M. *J. Am. Chem. Soc.* **1989**, *111*, 5959. (c) Johnson, G. K.; Schlemper, E. O. *J. Am. Chem. Soc.* **1978**, *100*, 3645. (d) Chen, L.; Jiang, F. L.; Lin, Z. Z.; Zhou, Y. F.; Yue, C. Y.; Hong, M. C. *J. Am. Chem. Soc.* **2005**, *127*, 8588. (e) Khan, M. I.; Zubieta, J. *Angew. Chem., Int. Ed.* **1994**, *33*, 760. (f) Salta, J.; Chen, Q.; Chang, Y. D.; Zubieta, J. *Angew. Chem., Int. Ed.* **1994**, *33*, 757.

(11) (a) Allis, D. G.; Rarig, R. S.; Burkholder, E.; Zubieta, J. *J. Mol. Struct.* **2004**, *688*, 11. (b) Allis, D. G.; Burkholder, E.; Zubieta, J. *Polyhedron* **2004**, *23*, 1145.

(12) (a) Tripathi, A.; Hughbanks, T.; Clearfield, A. *J. Am. Chem. Soc.* **2003**, *125*, 10528. (b) Liao, J. H; Juang, J. S.; Lai, Y. C. *Cryst. Growth Des.* **2006**, *6*, 354. (c) Lan, Y. Q.; Li, S. L.; Su, Z. M.; Shao, K. Z.; Ma, J. F.; Wang, X. L.; Wang, E. B. *Chem. Commun.* **2008**, 58.

(13) (a) Ballester, L.; Baxter, I.; Duncan, P. C. M.; Goodgame, D. M. L.; Grachvogel, D. A.; Williams, D. J. *Polyhedron* **1998**, *17*, 3613. (b) Ma, J. F.; Liu, J. F.; Xing, Y.; Jia, H. Q.; Lin, Y. H. *Dalton Trans.* **2000**, 2403. (c) Ma, J. F.; Yang, J.; Zheng, G. L.; Li, L.; Liu, J. F. *Inorg. Chem.* **2003**, *42*, 7531. (d) Cui, G. H.; Li, J. R.; Tian, J. L.; Bu, X. H.; Batten, S. R. *Cryst. Growth Des.* **2005**, *5*, 1775. (e) Yang, J.; Ma, J. F.; Liu, Y. Y.; Li, S. L.; Zheng, G. L. *Eur. J. Inorg. Chem.* **2005**, 2174. (f) Yang, J.; Ma, J. F.; Liu, Y. Y.; Ma, J. C.; Jia, H. Q.; Hu, N. H. *Eur. J. Inorg. Chem.* **2006**, 1208. (g) Wen, L. L.; Dang, D. B.; Duan, C. Y.; Li, Y. Z.; Tian, Z. F.; Meng, Q. J. *Inorg. Chem.* **2005**, *44*, 7161.

(14) (a) Zou, R. Q.; Liu, C. S.; Huang, Z.; Hu, T. L.; Bu, X. H. *Cryst. Growth Des.* **2006**, *6*, 99. (b) Peng, Y. F.; Ge, H. Y.; Li, B. Z.; Li, B. L.; Zhang, Y. *Cryst. Growth Des.* **2006**, *6*, 994. (c) Chen, C. L.; Goforth, A. M.; Smith, M. D.; Su, C. Y.; Zur Loye, H. C. *Inorg. Chem.* **2005**, *44*, 8762.

(15) (a) Dong, B. X.; Peng, J.; Gómez-García, C. J.; Benmansour, S.; Jia, H. Q.; Hu, N. H. *Inorg. Chem.* **2007**, *46*, 5933. (b) Dong, B. X.; Peng, J.; Zhang, P. P.; Tian, A. X.; Chen, J.; Xue, B. *Inorg. Chem. Commun.* **2007**, *10*, 839.

(16) Lan, Y. Q.; Li, S. L.; Wang, X. L.; Shao, K. Z.; Su, Z. M.; Wang, E. B. *Inorg. Chem.* **2008**, *47*, 529.

(17) Tian, A. X.; Ying, J.; Peng, J.; Sha, J. Q.; Han, Z. G.; Ma, J. F.; Su, Z. M.; Hu, N. H.; Jia, H. Q. *Inorg. Chem.* **2008**, *47*, 3274.

(18) Li, S. L.; Lan, Y. Q.; Ma, J. F.; Yang, J.; Wang, X. H.; Su, Z. M. *Inorg. Chem.* **2007**, *46*, 8283.

(19) Hill, C. L.; Renneke, R. *J. Am. Chem. Soc.* **1986**, *108*, 3528.

(20) Meng, X. R.; Song, Y. L.; Hou, H. W.; Han, H. Y.; Xiao, B.; Fan, Y. T.; Zhu, Y. *Inorg. Chem.* **2004**, *43*, 3528.

Scheme 2

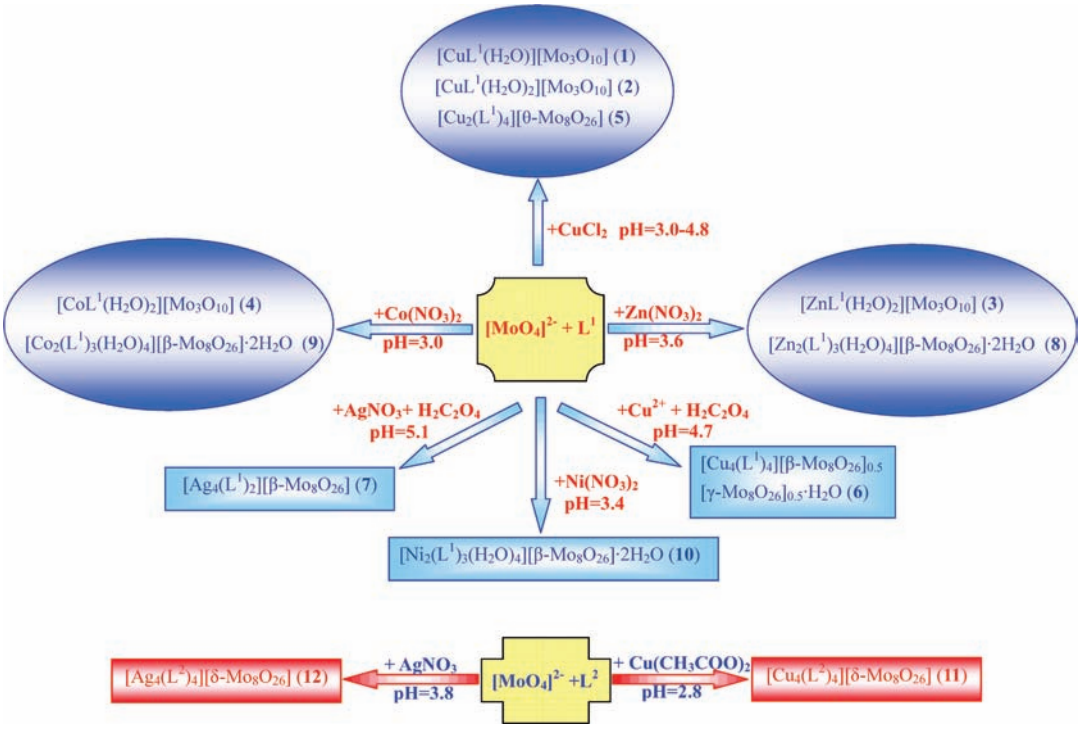

spectrometer. Elemental analyses (C, H, and N) were performed on a Perkin-Elmer 2400 CHN elemental analyzer. Powder X-ray diffraction (PXRD) data were collected with Cu Kα (λ = 1.5406 Å) radiation on a Rigaku X-ray diffractometer. Thermogravimetric analyses were carried out at a ramp rate of 5 °C min^{-1} in a helium atmosphere with a Shimadzu DTG-50 instrument. Emission spectra were recorded on a Perkin-Elmer LS50B luminescence spectrophotometer.

Syntheses. The hydrothermal syntheses were carried out in poly(tetrafluoroethylene)-lined stainless steel containers under autogenous pressure. The reaction vessel was filled to approximately 60% of its volume capacity.

Synthesis of $[CuL^1(H_2O)][Mo_3O_{10}]$ (1), $[CuL^1(H_2O)_2][Mo_3O_{10}]$ (2), and $[Cu_2(L^1)_4][Mo_8O_{26}]$ (5). H_2MoO_4 (0.1 g), $CuCl_2$ (0.06 g), L^1 (0.05 g), and H_2O (15 mL) in a molar ratio of 6:4:2:515 were mixed and stirred at room temperature for 30 min. The mixture was adjusted with 4 M HCl to pH 3.5 and then sealed in a Teflon-lined autoclave and heated at 170 °C for 5 days. After slow cooling to room temperature, glaucous blocklike **1** (yield: 5%), green needlelike **2** (yield: 40%), and blue blocklike **5** (yield: 30%) were obtained as a mixture. Compound **1** was obtained only once and could not be regenerated. There is no obvious influence of the initial pH value on the ratio of compounds **2** and **5** in the pH range of 3.5−4.8. However, the yield of compound **5** increases and that of compound **2** decreases in the pH range of 3.0−3.5. Furthermore, compound **5** can also be obtained as a single product but in polycrystalline form by heating the mixture of H_2MoO_4 (0.1 g), $Cu(NO_3)_2 \cdot 2H_2O$ (0.05 g), L^1 (0.05 g), and H_2O (15 mL) in a molar ratio of 6:2:2:515 at 170 °C for 5 days with a pH of 3.4 (yield: 85%). These crystals were filtered and hand-separated. IR (solid KBr pellet, cm^{-1}) of **1**: 3476 (m), 3109 (w), 1528 (m), 1428 (w), 1348 (w), 1287 (m), 1217 (w), 1125 (m), 1004 (w), 953 (s), 903 (s), 842 (w), 771 (w), 718 (m), 599 (m), 538 (w). IR of **2**: 3524 (w), 3318(w), 3144 (w), 1612 (m), 1530 (s), 1442 (w), 1381 (w), 1340 (w), 1290 (m), 1219(w), 1128(s), 1006(m), 903(s), 728(s), 597(s). Anal. calcd for $C_{12}H_{16}N_6CuMo_3O_{12}$: C, 18.30; H, 2.05; N, 10.67. Found: C, 18.69; H, 1.99; N, 10.87. IR of **5**: 3130 (m), 1625 (w), 1525 (s),1450 (m), 1420 (m), 1349 (w), 1278 (s), 1207 (s), 1123 (s), 1013 (m), 948 (s), 928 (s), 897 (s), 867 (s), 796 (m), 755 (m), 725 (m), 674 (s), 644 (m), 563 (w). Anal. calcd for $C_{48}H_{48}N_{24}Cu_2Mo_8O_{26}$: C, 25.37; H, 2.12; N, 14.79. Found: C, 25.21; H, 2.10; N, 14.77.

Synthesis of $[ZnL^1(H_2O)_2][Mo_3O_{10}]$ (3) and $[Zn_2(L^1)_3(H_2O)_4][Mo_8O_{26}] \cdot 2H_2O$ (8). A mixture of H_2MoO_4 (0.1 g), $Zn(NO_3)_2 \cdot 4H_2O$ (0.07 g), L^1 (0.05 g), and H_2O (15 mL) in a molar ratio of 6:2.5:2:515 was adjusted with HCl (4 M) to pH 3.6 and then sealed in a Teflon-lined autoclave and heated at 170 °C for 5 days. After slow cooling to room temperature, colorless needlelike crystals of **3** and blocklike crystals of **8** were filtered and hand-separated (yield: 50% and 30%, respectively). Compound **8** can also be synthesized as a single product using a modified process with a higher yield (80% based on Mo): H_2MoO_4 (0.12 g), $ZnSO_4 \cdot 7H_2O$ (0.06 g), L^1 (0.033 g), and H_2O (15 mL) in a molar ratio of 8:2:3:515 were mixed and adjusted to a pH of 3.4 and then sealed in the Teflon-lined autoclave and heated at 170 °C for 5 days. IR (solid KBr pellet, cm^{-1}) of **3**: 3527 (w), 3336 (m), 3139 (w), 1614 (m), 1528 (s),1435 (w), 1385 (w), 1344 (w), 1284 (s), 1213 (m), 1133 (s), 1014 (m), 1001 (m), 945 (m), 899 (s), 729 (s), 671 (s), 579 (s). Anal. calcd for $C_{12}H_{16}N_6ZnMo_3O_{12}$: C, 18.26; H, 2.04; N, 10.64. Found: C, 18.98; H, 1.87; N, 11.02. IR of **8**: 3293 (m), 3128 (w), 1630 (w), 1534 (m), 1442 (w), 1422 (w), 1361 (w), 1280 (m), 1210 (m), 1129 (m), 1027 (m), 997(m), 956 (s), 610 (s), 846 (s), 731 (s), 681 (s), 564 (m), 523 (m), 463 (w). Anal. calcd for $C_{36}H_{48}N_{18}Zn_2Mo_8O_{32}$: C, 20.18; H, 2.26; N, 11.76. Found: C, 20.28; H, 2.06; N, 11.93.

Synthesis of $[CoL^1(H_2O)_2][Mo_3O_{10}]$ (4) and $[Co_2(L^1)_3(H_2O)_4][Mo_8O_{26}] \cdot 2H_2O$ (9). A mixture of H_2MoO_4 (0.1 g), $Co(NO_3)_2 \cdot 6H_2O$ (0.06 g), L^1 (0.05 g), and H_2O (15 mL) in a molar ratio of 6:2:2:515 was adjusted with HCl (4 M) to a pH of 3.0 and then sealed in a Teflon-lined autoclave and heated at 170 °C for 5 days. After slow cooling to room temperature, red needlelike crystals of **4** and blocklike crystals of **9** were filtered and hand-separated (yield: 60% and 30%, respectively). Compound **4** can also be synthesized as a single product by heating a mixture of H_2MoO_4 (0.1 g), $CoCl_2 \cdot 6H_2O$ (0.07 g), L^1 (0.05 g), and H_2O (15 mL) in a molar ratio of 6:3:2:515 at 170 °C for 5 days at a pH of 3.3 (yield: 85%). IR (solid KBr pellet, cm^{-1}) of **4**: 3514 (w),

3309 (m), 3147 (w), 1617 (w), 1527(m), 1447(w), 1376 (w), 1346 (w), 1285(w), 1224(w), 1133 (m), 1022 (w), 1002 (w), 961 (m), 941 (m), 895 (s), 734 (s), 674 (s), 583(s). Anal. calcd for $C_{12}H_{16}N_6CoMo_3O_{12}$: C, 18.50; H, 1.55; N, 10.78. Found: C, 18.60; H, 2.01; N, 10.82. IR of **9**: 3306 (m), 3136 (w), 3115 (w), 1671 (w), 1630 (m), 1529 (m), 1440 (m), 1369 (m), 1339 (m), 1278 (m), 1217 (m), 1130 (s), 1027 (m), 996 (m), 963 (s), 912 (s), 841 (s), 731 (s), 678 (s), 650 (s), 567 (m), 516 (m), 466 (m). Anal. calcd for $C_{36}H_{48}N_{18}Co_2Mo_8O_{32}$: C, 20.29; H, 2.27; N, 11.83. Found: C, 20.22; H, 2.07; N, 11.92.

Synthesis of $[Cu_4(L^1)_4][Mo_8O_{26}]\cdot H_2O$ (6). A mixture of $Na_2MoO_4\cdot H_2O$ (0.2 g), $Cu(CH_3COO)_2\cdot H_2O$ (0.06 g), L^1 (0.05 g), $H_2C_2O_4$ (0.02 g), and H_2O (15 mL) in a molar ratio of 10:3:2:2:515 was adjusted with HCl (4 M) to a pH of 4.7 and then sealed in a Teflon-lined autoclave and heated at 170 °C for 5 days. After slow cooling to room temperature, brown blocklike crystals of **6** were filtered and washed with deioned water (80% yield based on Mo). IR (solid KBr pellet, cm^{-1}) of **6**: 3567 (w), 3445 (m), 3121 (s), 1615 (m), 1524(s), 1448(m), 1428 (m), 1387 (w), 1357(w), 1279(s), 1205 (m), 1125 (s), 1004 (s), 950 (s), 930 (m), 900 (m), 849 (s), 829 (m), 729 (s), 668 (m), 559(w), 519 (w), 428 (w). Anal. calcd for $C_{48}H_{50}N_{24}Cu_4Mo_8O_{27}$: C, 23.86; H, 2.09; N, 13.91. Found: C, 24.0; H, 1.97; N, 13.98.

Synthesis of $[Ag_4(L^1)_2][Mo_8O_{26}]$ (7). The preparation of **7** was similar to that of **6** except that $AgNO_3$ was used instead of $Cu(CH_3COO)_2\cdot H_2O$ and oxalic acid was not added. Colorless blocklike crystals of **7** were obtained at a pH of 5.1 with a 75% yield based on Mo. IR (solid KBr pellet, cm^{-1}) of **7**: 3450 (m), 3128 (w), 1628 (w), 1527 (m), 1456 (w), 1425 (w), 1375 (m), 1294 (m), 1273 (w), 1139 (m), 1048 (m),1008 (m), 945 (s), 901 (s), 843 (s), 710 (s), 670 (s), 629 (m), 547 (m). Anal. calcd for $C_{24}H_{24}N_{12}Ag_4Mo_8O_{26}$: C, 13.76; H, 1.15; N, 8.02. Found: C, 13.46; H, 1.08; N, 8.07.

Synthesis of $[Ni_2(L^1)_3(H_2O)_4][Mo_8O_{26}]\cdot 2H_2O$ (10). The synthesis of **10** was similar to that of **8** except that $Ni(CH_3COO)_2\cdot 4H_2O$ was used instead of $ZnSO_4\cdot 7H_2O$. The yield of green blocklike crystals of **10** at pH 3.4 is 65% based on Mo. IR (solid KBr pellet, cm^{-1}) of **10**: 3285 (m), 3148 (w), 3118 (w), 1674 (w), 1633 (w), 1529 (m), 1448 (m), 1428 (m), 1367 (w), 1336 (w), 1286 (m), 1215 (m), 1134 (m), 1031 (w), 1001 (w), 960 (s), 910 (s), 849 (s), 738 (m), 677 (s), 646 (s), 567 (m), 516 (m), 466 (w). Anal. calcd for $C_{36}H_{48}N_{18}Ni_2Mo_8O_{32}$: C, 20.30; H, 2.27; N, 11.84. Found: C, 20.72; H, 2.22; N, 12.04.

Synthesis of $[Cu_4(L^2)_4][Mo_8O_{26}]$ (11). A mixture of H_2MoO_4 (0.1 g), $Cu(CH_3COO)_2\cdot H_2O$ (0.06 g), L^2 (0.05 g), and H_2O (15 mL) in a molar ratio of 6:3:2:2:515 was adjusted with HCl (4 M) to a pH of 2.8 and then sealed in a Teflon-lined autoclave and heated at 170 °C for 5 days. After slow cooling to room temperature, brown blocklike crystals of **11** were filtered and washed with deioned water (40% yield based on Mo). IR (solid KBr pellet, cm^{-1}) of **11**: 3117 (m), 1523 (s), 1435 (m), 1392 (w), 1351 (w), 1291 (m), 1230 (m), 1108 (s), 1088 (s), 932 (m), 895 (s), 856 (m), 797 (s), 654 (s), 541 (w). Anal. calcd for $C_{56}H_{56}N_{16}Cu_4Mo_8O_{26}$: C, 28.13; H, 2.36; N, 9.37. Found: C, 28.10; H, 2.32; N, 9.34.

Synthesis of $[Ag_4(L^2)_4][Mo_8O_{26}]$ (12). The preparation of **12** was similar to that of **11** except that $AgNO_3$ was used instead of $Cu(CH_3COO)_2\cdot H_2O$. The optimized pH ranges for the synthesis of **12** is 3.8−5.0, and the yield of colorless blocklike crystals of **12** is 60% at a pH of 3.8 based on Mo. IR (solid KBr pellet, cm^{-1}) of **12**: 3123 (m), 1568 (m), 1537 (m), 1446 (w), 1396 (w), 1365 (w), 1274 (m), 1234 (m), 1183 (m), 1112 (s), 1092 (s), 931 (s), 901(m), 850 (w), 668 (s), 638 (s), 558 (m). Anal. calcd for $C_{56}H_{56}N_{16}Ag_4Mo_8O_{26}$: C, 26.19; H, 2.19; N, 8.72. Found: C, 26.11; H, 2.12; N, 8.66.

X-Ray Crystallography. Single-crystal X-ray diffraction data collections of complexes **1**−**12** were performed using an R-AXIS RAPID II diffractometer at 293 K with Mo Kα radiation (λ = 0.71073 Å). The structures were solved using direct methods and refined on F^2 using full-matrix least-squares methods using the SHELXTL package. Generally, the hydrogen atoms of the ligands were generated theoretically onto the specific atoms and refined isotropically with fixed thermal factors. The hydrogen atoms of water in complexes **1**, **4**−**5**, and **7**−**12** were located in difference Fourier maps, while the hydrogen atoms attached to water in compounds **2**−**3** and **6** were not located but were included in the structure factor calculations. A summary of the crystallographic data and structural determination for them is provided in Table 1. Selected bond lengths and bond length ranges of these compounds are listed in Table S1 (Supporting Information). Crystallographic data for the structures reported in this paper have been deposited in the Cambridge Crystallographic Data Center with CCDC numbers 692082−692093 for **1**−**12**.

Results and Discussion

Description of the Basic Building Blocks. By introducing the flexible ligands into the molybdate system, the $[Mo_3O_{10}]^{2-}$ isopolyoxoanion and four types (θ, β, γ, and δ) (Table 2) of $[Mo_8O_{26}]^{4-}$ (shortened as Mo_8) isomers are formed in complexes **1**−**12**. The $[Mo_3O_{10}]^{2-}$ subunit consists of three unsymmetrical distorted $[MoO_6]$ octahedra, which are in an edge- or corner-sharing arrangement.[21]

The θ-Mo_8 isomer is made up of four $[MoO_6]$ octahedra, two $[MoO_5]$ square pyramids, and two $[MoO_4]$ tetrahedra.[11] Herein, two pairs of edge-sharing $[MoO_6]$ octahedra and two $[MoO_5]$ square pyramids link together, forming a six-member ring through edge- and corner-sharing interactions. Two tetrahedral $[MoO_4]$ subunits cap on either face of the ring in a corner-sharing mode. Thus, the θ isomer exhibits fourteen terminal, eight doubly bridging, and four triply bridging oxo groups.

The β-Mo_8 isomer consists of eight edge-sharing $[MoO_6]$ octahedra with two $[Mo_4O_{13}]$ subunits stacking together.[22] Thus, the β isomer contains fourteen terminal, six doubly bridging, four triply bridging, and two five-fold bridging oxo groups.

The γ-Mo_8 isomer is closely related to the θ isomer in that it exhibits the same six-membered ring as that of the θ-Mo_8. However, in the γ isomer, the capping subunit on either face of the ring is the $[MoO_5]$ square pyramid in the edge-sharing mode. Such an arrangement produces fourteen terminal, six doubly bridging, four triply bridging, and two four-fold bridging oxo groups.[23]

The δ-Mo_8 isomer is composed of four $[MoO_6]$ octahedra and four $[MoO_4]$ tetrahedra.[24] Two pairs of edge-sharing $[MoO_6]$ octahedra and two $[MoO_4]$ tetrahedra connect alternately, forming another type of six-membered ring, and then, the other two $[MoO_4]$ tetrahedra cap on either face of the ring in the corner-sharing mode so as to construct δ-$[Mo_8O_{26}]^{4-}$. A total of fourteen terminal, ten doubly bridging, and two triply bridging oxo groups are included in this type of isomer.

The Mo−O lengths in these complexes are in the normal ranges (Table S1, Supporting Information).

(21) Sun, D. H.; Zhang, H. J.; Zhang, J. L.; Zheng, G. L.; Yu, J. B.; Gao, S. Y. *J. Solid State Chem.* **2007**, *180*, 393.
(22) Chen, S. M.; Lu, C. Z.; Yu, Y. Q.; Zhang, Q. Z.; He, X. *Inorg. Chem. Commun.* **2004**, *7*, 1041.
(23) DeBord, J. R. D.; Haushalter, R. C.; Meyer, L. M.; Rose, D. J.; Zapf, P. J.; Zubieta, J. *Inorg. Chim. Acta* **1997**, *256*, 165.
(24) Hagrman, D.; Zubieta, C.; Haushalter, R. C.; Zubieta, J. *Angew. Chem., Int. Ed. Engl.* **1997**, *36*, 873.

Table 1. Crystal Data and Structure Refinement for Compounds **1**−**12**

	1	**2**	**3**	**4**	**5**	**6**
empirical formula	$C_{12}H_{14}N_6CuMo_3O_{11}$	$C_{12}H_{16}N_6CuMo_3O_{12}$	$C_{12}H_{16}N_6ZnMo_3O_{12}$	$C_{12}H_{12}N_6CoMo_3O_{12}$	$C_{48}H_{48}N_{24}Cu_2Mo_8O_{26}$	$C_{48}H_{50}N_{24}Cu_4Mo_8O_{27}$
fw	769.68	787.66	789.50	783.06	2271.7	2416.8
temp (K)	293(2)	293(2)	293(2)	293(2)	293(2)	293(2)
wavelength (Å)	0.71073	0.71073	0.71073	0.71073	0.71073	0.71073
cryst syst	triclinic	monoclinic	monoclinic	monoclinic	monoclinic	triclinic
space group	$P\bar{1}$	$P2_1/c$	$P2_1/c$	$P2_1/c$	$P2_1/c$	$P\bar{1}$
a (Å)	8.0600(16)	8.1300(16)	8.1800(16)	8.1800(16)	12.400(3)	11.900(2)
b (Å)	8.9000(18)	29.670(6)	29.900(6)	30.000(6)	15.300(3	13.700(3)
c (Å)	14.400(3)	8.900(18)	8.8900(18)	8.8500(18)	20.090(4)	23.640(5)
α (deg)	92.20(3)					104.36(3)
β (deg)	99.70(3)	102.70(3)	104.06(3)	104.20(3)	103.70(3)	91.70(3)
γ (deg)	103.60(3)					109.63(3)
volume (Å ^{3})	986.4(3)	2094.3 (7)	2109.2(7)	2105.4(7)	3703.0(13)	3489.6(12)
Z	2	4	4	4	2	2
D_{calcd} (mg/m^3)	2.591	2.498	2.486	2.470	2.037	2.300
abs coeff (mm^{-1})	3.001	2.834	2.942	2.596	1.958	2.674
F (000)	742	1524	1528	1516	2212	2348
θ for data collection (deg)	3.08−27.66	3.12−24.00	3.11−27.52	3.12−27.51	3.15−27.50	3.06−25.00
limiting indices	$-10 \le h \le 10$, $-11 \le k \le 11$, $-17 \le l \le 18$	$-9 \le h \le 9$, $-33 \le k \le 33$, $-9 \le l \le 10$	$-11 \le h \le 11$, $-38 \le k \le 38$, $-9 \le l \le 10$	$-11 \le h \le 11$, $-38 \le k \le 38$, $-10 \le l \le 10$	$-16 \le h \le 16$, $-19 \le k \le 19$, $-26 \le l \le 26$	$-14 \le h \le 14$, $-16 \le k \le 16$, $-27 \le l \le 28$
reflns collected/ unique	9801/4540	14044/ 3280	20058/4856	20418/4842	34402/8468	26362/ 11872
unique reflns (R_{int})	0.0378	0.0725	0.0529	0.0264	0.0574	0.0517
goodness-of-fit on F^2	1.086	1.330	1.129	0.998	1.107	1.003
final R indices [$I > 2\sigma(I)$]	$R_1 = 0.0346$, $wR_2 = 0.0981$	$R_1 = 0.0998$, $wR_2 = 0.2474$	$R_1 = 0.0438$, $wR_2 = 0.1122$	$R_1 = 0.0220$, $wR_2 = 0.0515$	$R_1 = 0.0436$, $wR_2 = 0.1031$	$R_1 = 0.0439$, $wR_2 = 0.1270$
R indices (all data)	$R_1 = 0.0369$, $wR_2 = 0.0995$	$R_1 = 0.1037$, $wR_2 = 0.2490$	$R_1 = 0.0494$, $wR_2 = 0.1162$	$R_1 = 0.0265$, $wR_2 = 0.0550$	$R_1 = 0.0574$, $wR_2 = 0.1111$	$R_1 = 0.0780$, $wR_2 = 0.1761$

	7	**8**	**9**	**10**	**11**	**12**
empirical formula	$C_{24}H_{24}N_{12}Ag_4Mo_8O_{26}$	$C_{36}H_{48}N_{18}Zn_2Mo_8O_{32}$	$C_{36}H_{48}N_{18}Co_2Mo_8O_{32}$	$C_{36}H_{48}N_{18}Ni_2Mo_8O_{32}$	$C_{56}H_{56}N_{16}Cu_4Mo_8O_{26}$	$C_{56}H_{56}N_{16}Ag_4Mo_8O_{26}$
fw	2095.55	2143.18	2130.30	2129.92	2390.86	2568.15
temp (K)	293(2)	293(2)	293(2)	293(2)	293(2)	293(2)
wavelength (Å)	0.71073	0.71073	0.71073	0.71073	0.71073	0.71073
cryst syst	triclinic	triclinic	triclinic	triclinic	monoclinic	monoclinic
space group	$P\bar{1}$	$P\bar{1}$	$P\bar{1}$	$P\bar{1}$	$P2_1/n$	$P2_1/n$
a (Å)	9.2800(19)	10.200(2)	10.200(2)	10.100(2)	12.740(3)	12.700(3)
b (Å)	10.750(2)	12.650(3)	12.600(3)	12.650(3)	22.950(5)	23.150(5)
c (Å)	11.890(2)	13.108(3)	13.100(3)	13.047(3)	13.030(3)	13.200(3)
α (deg)	77.91(3)	89.62(3)	79.20(3)	89.15(3)		
β (deg)	74.46(3)	67.54(3)	67.10(3)	67.55(3)	109.03(3)	108.10(3)
γ (deg)	80.58(3)	74.70(3)	74.70(3)	74.80(3)		
volume (Å ^{3})	1110.1(4)	1499.2(5)	1489.1(5)	1480.0(5)	3601.5(15)	3688.8(13)
Z	1	1	1	1	2	2
D_{calcd} (mg/m^3)	3.135	2.374	2.362	2.390	2.205	2.312
abs coeff (mm^{-1})	4.001	2.505	2.273	2.363	2.585s	2.433
F (000)	984	1042	1024	1038	2328	2472
θ for data collection (deg)	3.18−25.00	3.05−27.50	3.05−25.00	3.07−27.68	3.13−25.00	3.10−25.00
limiting indices	$-10 \le h \le 11$, $-12 \le k \le 12$, $-14 \le l \le 14$	$-13 \le h \le 11$, $-16 \le k \le 16$, $-16 \le l \le 17$	$-12 \le h \le 10$, $-14 \le k \le 14$, $-15 \le l \le 15$	$-13 \le h \le 13$, $-16 \le k \le 16$, $-16 \le l \le 16$	$-15 \le h \le 14$, $-26 \le k \le 27$, $-15 \le l \le 15$	$-15 \le h \le 13$, $-26 \le k \le 27$, $-15 \le l \le 15$
reflns collected/ unique	8768/3896	14775/6802	11560/5202	14390/6705	27668/6340	27215/6400
unique reflns (R_{int})	0.0271	0.0228	0.0323	0.0243	0.0232	0.0966
goodness-of-fit on F^2	1.183	1.121	1.070	1.117	1.025	1.054
final R indices [$I > 2\sigma(I)$]	$R_1 = 0.0273$, $wR_2 = 0.0868$	$R_1 = 0.0279$, $wR_2 = 0.0856$	$R_1 = 0.0383$, $wR_2 = 0.1128$	$R_1 = 0.0263$, $wR_2 = 0.0835$	$R_1 = 0.0319$, $wR_2 = 0.1150$	$R_1 = 0.0591$, $wR_2 = 0.1474$
R indices (all data)	$R_1 = 0.0409$, $wR_2 = 0.1253$	$R_1 = 0.0386$, $wR_2 = 0.1062$	$R_1 = 0.0481$, $wR_2 = 0.1242$	$R_1 = 0.0343$, $wR_2 = 0.0916$	$R_1 = 0.0370$, $wR_2 = 0.1197$	$R_1 = 0.1190$, $wR_2 = 0.2115$

Structural Analyses. $[CuL^1(H_2O)][Mo_3O_{10}]$ (1). The single-crystal XRD reveals that compound **1** is constructed from the 2D neutral sheet $[Cu(H_2O)Mo_3O_{10}]$, pillared by the L^1 subunits into a 3D isopolymolybdate framework. As shown in Figure 1a, in the asymmetry unit, all of the three unique Mo^{VI} centers adopt the

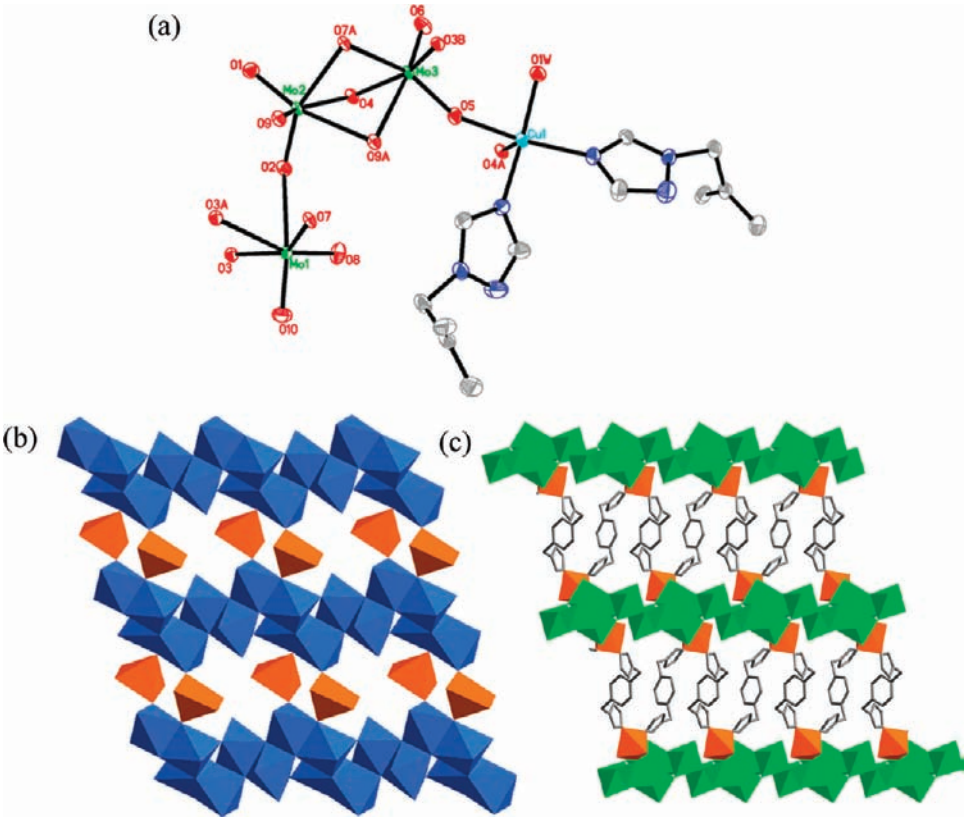

Figure 1. (a) ORTEP drawing of **1** at the 50% probability level, showing the coordination environments around Cu and Mo atoms. All hydrogen atoms are omitted for clarity in this and the following figures. (b) Polyhedral representation of the layer in **1**. (c) Illustration of the pillar-layered framework of **1**.

Table 2. Summary of the Structural Characteristics of Four Types of Octamolybdate in Compounds **1**−**12**

Type of $[Mo_8O_{26}]^{4-}$ isomers	θ	β	γ	δ
Polyhedral representation of the octamolybdate structures				
Polyhedral subunits	4 octahedra 2 square pyramids 2 tetrahedra	8 octahedra	6 octahedra 2 square pyramids	4 octahedra 4 tetrahedra
Oxo-group types	14t, $8\mu_2$, $4\mu_3$	14t, $6\mu_2$,$4\mu_3$, $2\mu_5$	14t, $6\mu_2$, $4\mu_3$,$2\mu_4$	14t,$10\mu_2$,$2\mu_3$

distorted $[MoO_6]$ octahedral geometry, and the Cu^{II} center exhibits the $[CuN_2O_3]$ square-pyramidal configuration, which is coordinated by two nitrogen atoms from the triazole rings of two L^1 groups, two oxygen atoms from two $[Mo_3O_{10}]$ trimers, and one oxygen atom from the coordinated water molecule.

In the $[Mo_3O_{10}]$ trimer, the $[Mo(1)O_6]$ octahedron is connected to the $[Mo(3)O_6]$ octahedron by a shared edge. Octahedra $[Mo(3)O_6]$ and $[Mo(2)O_6]$ are connected by two shared edges. Each trimer unit is then joined up with another symmetry-related moiety by sharing one edge and two corners to form a unit of six octahedra (see Figure S1, Supporting Information). The hexamer units are connected together by sharing edges ($[Mo(1)O_6]$ octahedra) to form an infinite chain. In the *ab* plane, the adjacent inorganic chains are connected through the $[CuN_2O_3]$ square pyramids by sharing oxygen atoms of O(4) and O(5) to form the 2D sheet (Figure 1b). The distance between the adjacent chains is ca. 2.95 Å, represented by the O···O separation through the O(4)−Cu−O(5) linkage. The bond angle of ∠O(4)−Cu−O(5) is about 89.87°, as shown in Figure S2a (Supporting Information). The L^1 molecules exhibit the Z-shaped conformation and connect the neutral sheets to form a 3D pillar-layered framework (see Figure 1c).

$[ML^1(H_2O)_2][Mo_3O_{10}]$ [M = Cu (2), Zn (3), and Co (4)]. As revealed by the single-crystal XRD, compounds **2**−**4** are isostructural and crystallize in the monoclinic $P2_1/c$ space group. The structure of **2** will be discussed in detail as an example. The coordination environment around the Cu^{II} and Mo^{VI} centers is shown in Figure 2a. Complex **2** exhibits a similar $[Mo_3O_{10}]$ trimer and $[Mo_3O_{10}]_n^{2n-}$ infinite chain to those in complex **1** (see Figure S3, Supporting Information). It should be noted

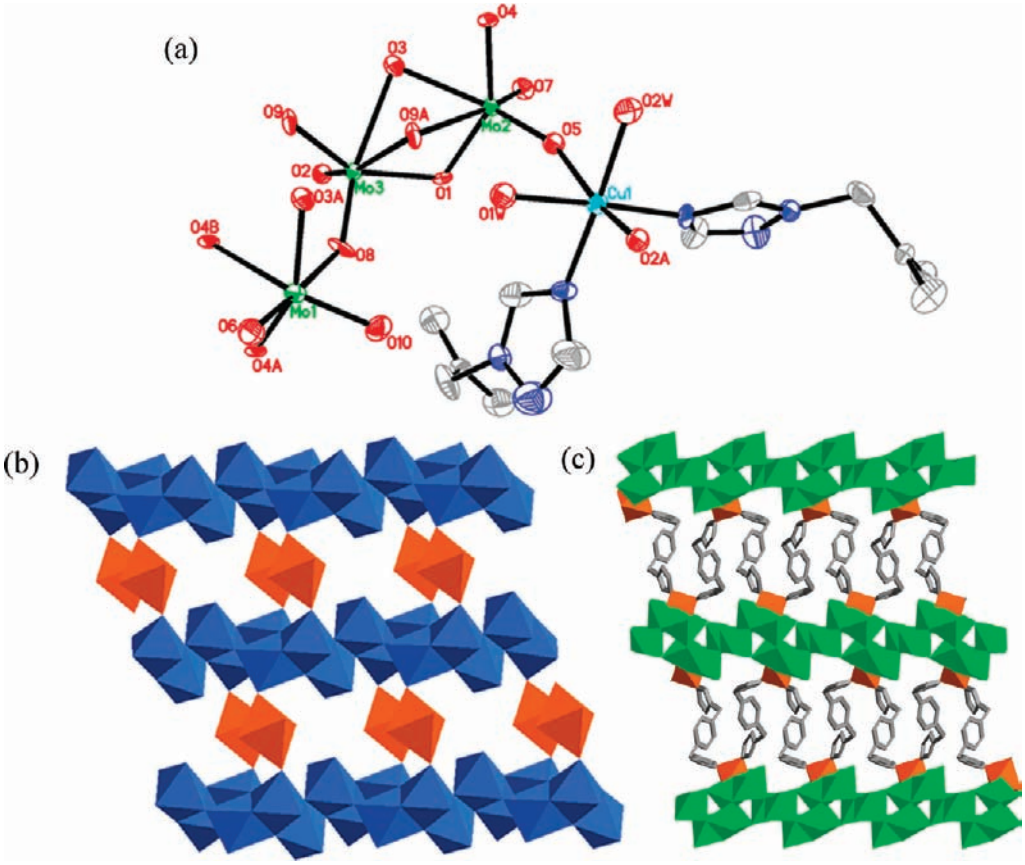

Figure 2. (a) ORTEP drawing of **2** at the 50% probability level, showing the coordination environments around Cu and Mo atoms. (b) Polyhedral representation of the 2D sheet in **2**. (c) Illustration of the pillar-layered framework of **2**.

that the significant difference between **1** and **2** is the coordination environment around the Cu^{II}. In complex **2**, the Cu^{II} center is surrounded by two nitrogen atoms from the triazole rings of two symmetry-related L^1 groups, two oxygen atoms from two $[Mo_3O_{10}]$ trimers, and two coordinated water molecules, forming a $[CuN_2O_4]$ octahedron. Adjacent $[Mo_3O_{10}]_\infty$ inorganic chains share oxygen atoms O(2) and O(5) with the $[CuN_2O_4]$ octahedra forming the neutral $[Cu(H_2O)_2Mo_3O_{10}]$ oxide layer in the *ac* plane (Figure 2b). Different from **1**, the shared oxygen atoms O(2) and O(5) in complex **2** lie in two axial positions in the octahedral configuration. Thus, complex **2** exhibits a bigger bond angle of $\angle$O(2)−Cu−O(5) = 160.51° and a longer distance of 4.245 Å between the adjacent chains represented by the O(2)···O(5) separation (Figure S2b, Supporting Information). The Z-shaped L^1 molecules pillar the adjacent layers and give rise to the formation of a 3D framework (Figure 2c).

$[Cu_2(L^1)_4][Mo_8O_{26}]$ (5). Compound **5** consists of two Cu^{2+} ions, four L^1 ligands, and one θ-type Mo_8 polyoxoanion (Figure 3a). Each Cu^{II} center is surrounded by four equatorial nitrogen atoms (N(1), N(4), N(7), and N(10)) from two L^1 molecules and two trans-oxygen atoms (O(6) and O(11)) from two neighboring Mo_8 clusters in an octahedral geometry (Cu−N = 1.994(4)−2.018(4) Å, Cu−O = 2.373(3)−2.609(4) Å). Each Mo_8 cluster is covalently bonded to four Cu^{II} via four terminal oxygen atoms of the cluster. Interestingly, the Cu^{II} centers are bridged by one set of V-shaped L^1 molecules to form the left- and right-handed helical chains running along a crystallographic 2_1 axis in the *b* direction with a pitch of ca. 15.0 Å (Figure S4a, Supporting Information). The adjacent helical chains are interconnected by the Mo_8 clusters to generate a 2D layer with quadrate windows (ca. 8.9 Å × 5.3 Å), as shown in Figure 3b. Note that these 2D layers are further extended into a 3D pillar-layered framework by another set of left- and right-handed helical chains, which are constructed by the Z-shaped L^1 molecules (see Figure 3c and Figure S4b, Supporting Information). The pitch of the pillared helical chains is about 27.9 Å.

$[Cu_4(L^1)_4][Mo_8O_{26}]\cdot H_2O$ (6). Single-crystal XRD reveals that **6** has a complicated polythread penetrated double-ladder structure. There are five crystallographically independent Cu^I centers in the asymmetric unit, in which Cu(4) and Cu(5) are half-occupied (see Figure S5, Supporting Information). Cu(1), Cu(4), and Cu(5) centers display a linear coordination mode and are coordinated by two nitrogen atoms from two L^1 molecules. All Cu(1) centers are joined together by the L^1 molecules to generate an infinite $[Cu\text{-}L^1]_n$ thread (labeled as thread A). The alternate Cu(4) and Cu(5) centers are also linked together by L^1 to form another $[Cu\text{-}L^1]_n$ thread (labeled as thread B).

In addition, Cu(2) and Cu(3) centers are coordinated by two nitrogen atoms from two L^1 molecules and one oxygen atom from the Mo_8 cluster, exhibiting T-shaped coordination geometry. Note that there are two types of Mo_8 anions, namely, β-Mo_8 and γ-Mo_8, coexisting in this compound. Interestingly, the two types of Mo_8 anions, functioning as the rungs, bridge two sets of $[Cu\text{-}L^1]_n$

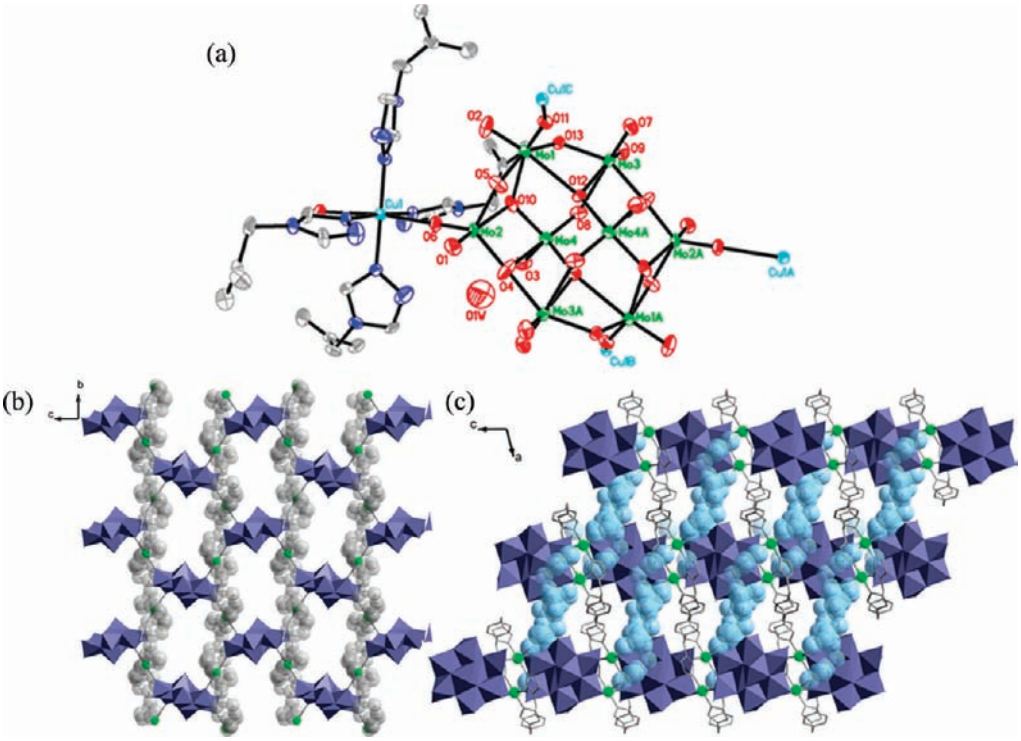

Figure 3. (a) ORTEP drawing of **5** at the 50% probability level, showing the coordination environments around Cu and Mo atoms. (b) Illustration of the 2D sheet constructed by helical chains. (c) View of the pillar-layered framework of **5**.

polymeric single chains made from Cu(2)-L^1 and Cu(3)-L^1 fragments, respectively, to form two types of ladderlike double chains of $[Cu(2)(L^1)(\gamma\text{-}Mo_8)_{0.5}]_n^{n-}$ (labeled as ladder A) and $[Cu(3)(L^1)(\beta\text{-}Mo_8)_{0.5}]_n^{n-}$ (labeled as ladder B), as shown in Figure 4a and b. The Cu(2) center shares one μ_2-O of O(15) with the γ-Mo_8 whereas the Cu(3) center shares one terminal oxygen atom of O(6) with the β-Mo_8 cluster. The Cu−O bond lengths are 2.671(8) and 2.622(3) Å, respectively.

The most fascinating structural feature of **6** is that those two ladders, ladder A and ladder B, are penetrated respectively by single-stranded thread B and double-stranded thread A in an inclined way. Two such types of polythread-penetrated subunits array alternately in a crosslike fashion (Figure 4c). It is unprecedented to the best of our knowledge that two sorts of polyoxoanions coexist in one structure, inducing the formation of two sorts of ladderlike building blocks and finally the polythread structure. All of the L^1 molecules in the $[Cu\text{-}L^1]_n$ polymeric chains exhibit the Z-shaped conformation.

$[Ag_4(L^1)_2][Mo_8O_{26}]$ (7). The single-crystal XRD analysis shows that compound **7** contains the β-$[Mo_8O_{26}]$ unit as the main building block. As mentioned above, the β-Mo_8 cluster consists of two $[Mo_4O_{13}]$ subunits in which each one exhibits an $[O_4]$ unit of four terminal oxygen atoms in a square-planar arrangement. As seen from Figure 5a, each crystallographically half-occupied $Ag^I(3)$ center in **7** binds to two $[O_4]$ faces of two adjacent Mo_8 clusters through six Ag−O coordinative bonds (Ag−O bond length in the range of 2.46(3)−2.71(3) Å) and two Ag−O contacts (Ag−O distances of 2.756(3) and 2.903(3) Å), forming an infinite chain of $[AgMo_8O_{26}]_n^{3n-}$ (Figure 5b). Interestingly, such a coordination style of Ag^I is rare, and the role of the Ag(3) atom in the infinite chain is similar to that of the $[Ag_2]$ dimer in the complex $[Ag(C_7H_{12}O_2N)(CH_3CN)]_{2n}[Ag_2(CH_3CN)_2(Mo_8O_{26})]_n \cdot 2CH_3CN$,[25] in which the polymeric chain is obtained thanks to the formation of the Ag−Ag bonds and the long-range Ag−O contacts (Ag−O distances of 2.8−2.9 Å). The Ag^I coordination sphere in the latter is filled by an $[O_4]$ unit of one β-Mo_8 cluster, one CH_3CN molecule, and two terminal oxygen atoms in the $[O_4]$ face of another β-Mo_8 cluster (see Figure S6a, Supporting Information).

Another interesting feature of **7** is the connection style of the cationic $[Ag_3(L^1)_2]^{3+}$ fragment. Every two Ag(1) centers is connected through two Z-shaped L^1 molecules to form a dinuclear molecular loop of $[Ag(1)_2(L^1)_2]^{2+}$. One terminal N atom and one N−N bridging N atom at the two ends of the L^1 molecule join the coordination with Ag(1). Extension of the $[Ag(1)_2(L^1)_2]^{2+}$ loop through the coordination of another terminal N atom of the L^1 ligand with the crystallographically half-occupied Ag(2) center generates a 1D polymeric chain $[Ag_3(L^1)_2]_n^{3n+}$, as shown in Figure 5c. In the lattice, the inorganic polymeric chains $[AgMo_8O_{26}]_n^{3-}$ and organic polymeric chains $[Ag_3(L^1)_2]_n^{3n+}$ are interlaced and interact together via C−H···O short contacts (Figure S6b, Supporting Information).

$[M_2(L^1)_3(H_2O)_4][Mo_8O_{26}] \cdot 2H_2O$ [M = Zn (8), Co (9), and Ni (10)]. Single-crystal XRD analysis reveals that compounds **8**−**10** are isostructural and crystallize in the triclinic $P\bar{1}$ space group. Only the structure of **8** will be described in detail as an example. Compound **8** is constructed from one β-type Mo_8 polyoxoanion, two Zn^{2+} ions, three L^1 molecules, four coordinated water molecules, and two lattice water molecules (Figure 6a). The

(25) Abbas, H.; Streb, C.; Pickering, A. L.; Neil, A. R.; Long, D. L.; Cronin, L. *Cryst. Growth Des.* **2008**, *8*, 635.

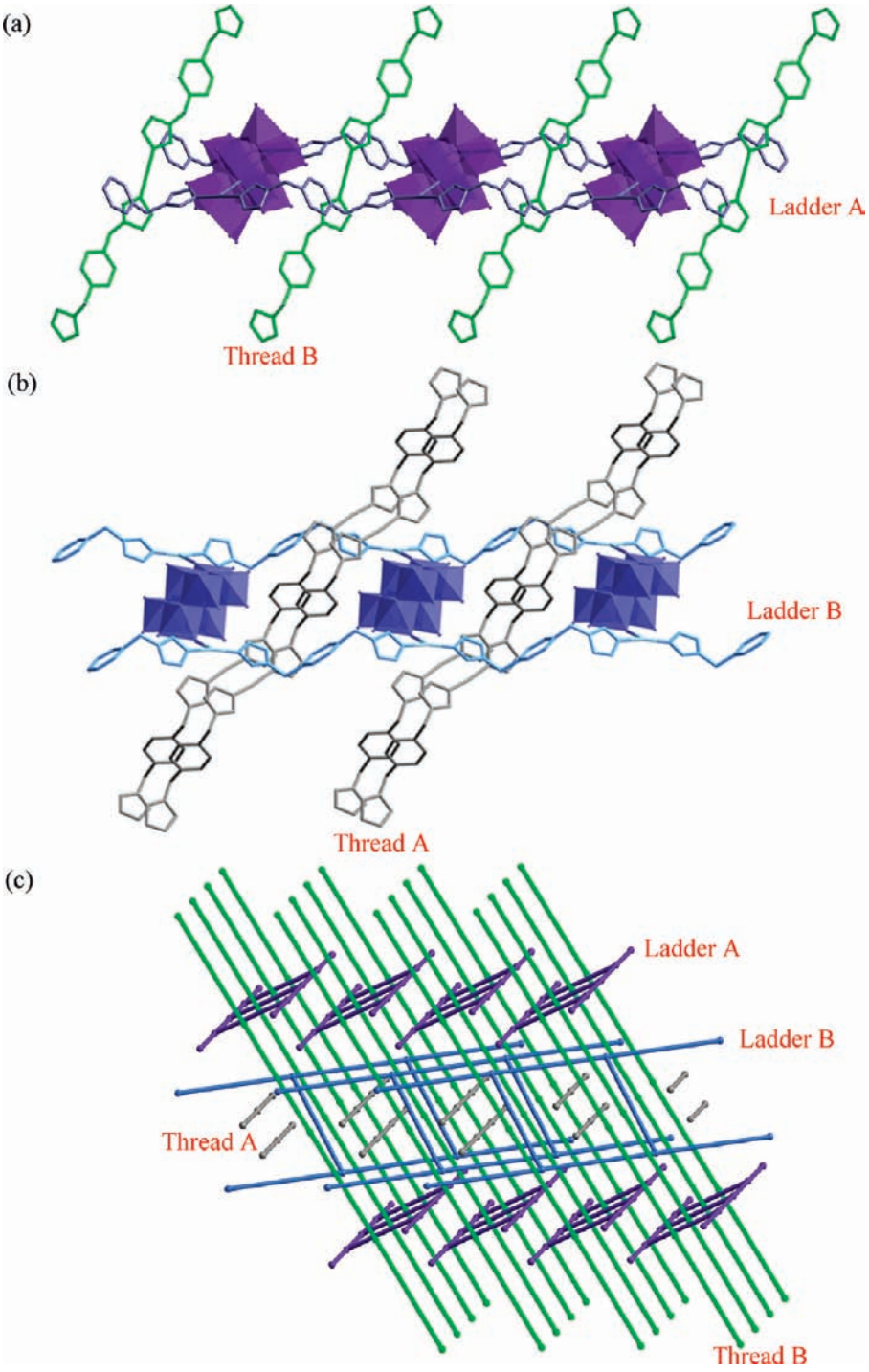

Figure 4. View of the two types of ladderlike double chains of ladder A (a) and ladder B (b) as well as the schematic representation (c) of the polythread penetrated structure in **6**.

coordination sphere of each Zn atom is achieved by three nitrogen atoms from three L^1 molecules, one terminal oxygen atom from one β-Mo_8 cluster, and two water molecules. Interestingly, there also exists one type of $[Zn_2(L^1)_2]^{4+}$ dinuclear molecular loop in **8** which has two L^1 molecules in a V-shaped conformation. Each Mo_8 cluster is covalently bonded to two $[Zn_2(L^1)_2]^{4+}$ loops via the Zn−O coordinative bonds and thereby generates a 1D extension, as shown in Figure 6b. The Z-shaped L^1 molecules arrange perpendicularly to the direction of the chain propagation and therefore extend the chains into the network. The big cavity of such a network is about 23.1 Å × 13.7 Å. In order to keep the structure tighter, two such nets penetrate each other, forming a parallel two-fold (2D → 2D) interpenetrated network structure, as shown in Figure 6c. Furthermore, the adjacent layers interact via $\pi\cdots\pi$ interactions and C−H···O short contact interactions.

$[M_4(L^2)_4][Mo_8O_{26}]$ [M = Cu (11) and Ag (12)]. Compounds **11** and **12** are isostructural, and they have 3D polythread penetrated frameworks based on the δ-Mo_8 anion. Herein, we will lay the emphasis on the structure of

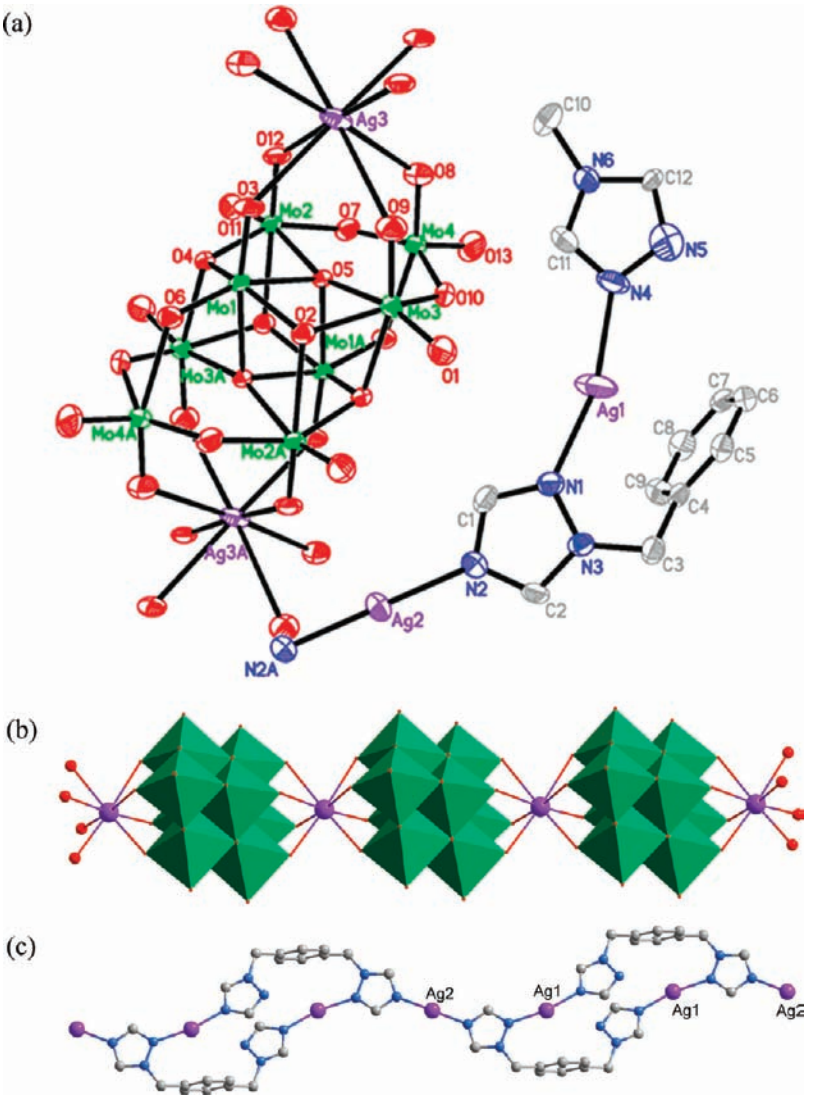

Figure 5. (a) ORTEP drawing of **7** at the 50% probability level, showing the coordination environments around Ag and Mo atoms. (b) Polyhedral representation of the inorganic $\{AgMo_8O_{26}\}_{3n}^{3-}$ chain in **7**. (c) View of the organic polymeric chains $\{Ag_3(L^1)_2\}_n^{3n+}$ in **7**.

11. Compound **11** has two crystallographically independent Cu^I centers, Cu(1) and Cu(2). The Cu(1) center exhibits linear geometry, which is coordinated by two nitrogen atoms from two L^2 molecules, while the Cu(2) center is four-coordinated by two nitrogen atoms from two L^2 molecules and two oxygen atoms from two δ-Mo_8 anions in a seesaw style (see Figure 7a). Each δ-Mo_8 anion is covalently bonded to four Cu(2) centers, and as a result, a 2D sheet is formed through such a connection style, as shown in Figure S7a (Supporting Information). Furthermore, the L^2 2-connectors ligated in the Cu(2) centers support such a 2D sheet to form a 3D pillared framework (Figure 7b). Interestingly, there are quadrate, rhombic, and tetragonal channels in the *ac* plane, [101] plane, and *ab* plane, respectively. The openings of these channels are ca. 7.2 Å × 7.0 Å, 7.0 Å × 9.5 Å, and 7.3 Å × 6.2 Å, respectively (Figure S7b–d, Supporting Information). Note that, among these channels, we find the wavelike chains constructed by Cu(1) and L^2 molecules. These wavelike chains extend along the *b* axis and penetrate between the two adjacent quadrate channels. Moreover, the L^2 molecules ligated in the Cu(1) and Cu(2) centers exhibit V-shaped and Z-shaped conformations, respectively.

Discussion. As demonstrated in the Experimental Section, all of the compounds **1**–**12** were obtained by acidifying the $[MoO_4]^{2-}$ aqueous solution. We tentatively deduce the conversion pathways of the $[MoO_4]^{2-}$ anion into the $[Mo_3O_{10}]^{2-}$ and $[Mo_8O_{26}]^{4-}$ anions according to the following acid–base equilibria (eqs 1 and 2):

$$3[MoO_4]^{2-} + 4H^+ \rightarrow [Mo_3O_{10}]^{2-} + 2H_2O \quad (1)$$

$$8[MoO_4]^{2-} + 12H^+ \rightarrow [Mo_8O_{26}]^{4-} + 6H_2O \quad (2)$$

In addition, compounds **1**, **2** and **5**, **3** and **8**, and **4** and **9** are concomitant mutually, which suggests that there may exist some relationship between the $[Mo_3O_{10}]^{2-}$ and $[Mo_8O_{26}]^{4-}$ anions (eq 3). Such an equilibrium has also been proposed by Jobic et al. in the molybdate system containing organoammonium cations as the structure-directing reagent.[26]

$$8[Mo_3O_{10}]^{2-} + 4H^+ \leftrightarrow 3[Mo_8O_{26}]^{4-} + 2H_2O \quad (3)$$

(26) Coué, V.; Dessapt, R.; Bujoli-Doeuff, M.; Evain, M.; Jobic, S. *Inorg. Chem.* **2007**, *46*, 2824.

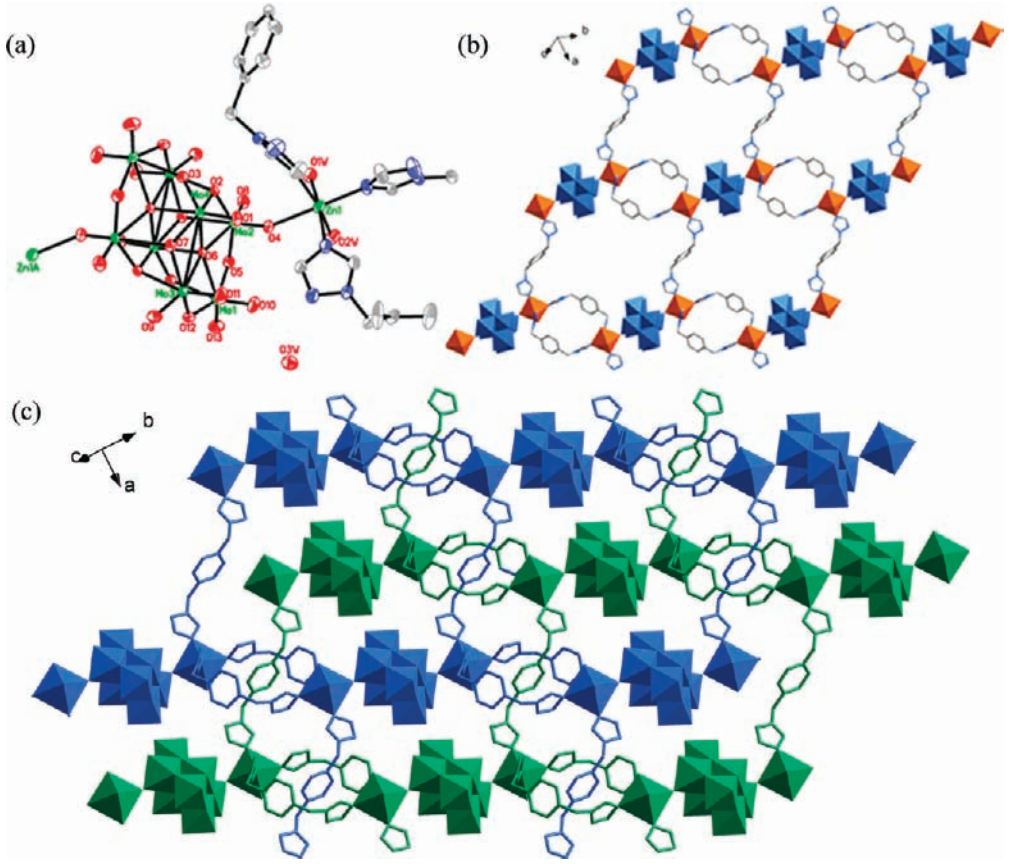

Figure 6. (a) ORTEP drawing of **8** at the 50% probability level, showing the coordination environments around Zn and Mo atoms. (b) View of the 2D sheet constructed by $[Zn_2(L^1)_2]^{4+}$ loops and β-Mo_8 polyoxoanions. (c) View of the parallel two-fold interpenetrated network structure of **8**.

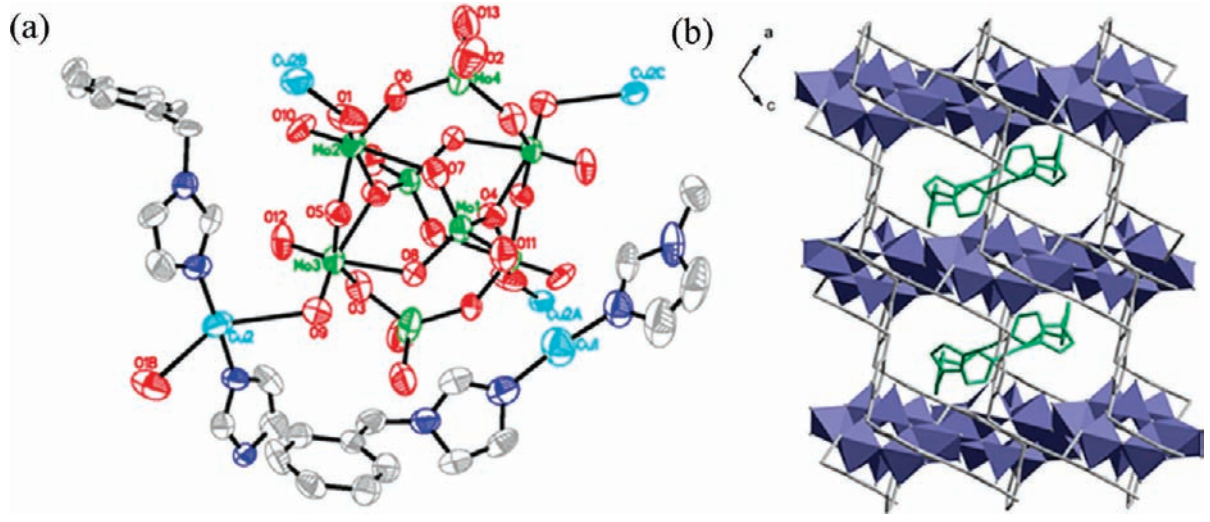

Figure 7. (a) ORTEP drawing of **11** at the 50% probability level, showing the coordination environments around Cu and Mo atoms. View of the 3D pillar-layered structure of **11** without (b) and with (c) the $\{Cu\text{-}L^2\}_n^{n+}$ wavelike chain in the channels.

As shown in Scheme S1 (Supporting Information), six compounds (compounds **5**−**10**) based on ML^1 and $[Mo_8O_{26}]^{4-}$ clusters were successfully synthesized. For the compounds containing divalent transition metal ions, that is, **5**, **8**−**10**, although all of the M^{II} in them take on the six-coordinated octahedral geometry, different donor sets of $[N_4O_2]$ and $[N_3O_3]$ occur in **5** ($M = Cu^{II}$) and **8**−**10** ($M = Zn^{II}$, Co^{II}, and Ni^{II}), respectively. By investigating the previous reports about $[Mo_8O_{26}]^{4-}$ clusters, we found that the β isomer is the most prevalent existing form in the octamolybdate-based hybrids that is coordinated by a divalent transition metal complex.[11] However, obviously, compound **5** is an exceptive example, which shows a four-connected θ-type isomeric form instead. Such an exception may be ascribed to the special coordination behavior of the Cu^{II} cation, which tends to form an elongated octahedral geometry due to the strong Jahn−Teller effect of its d^9 electronic configuration (Figure S8, Supporting Information). As a result, the Cu^{II} cation takes on two long Cu−O bonds (2.373(3) and 2.609(4) Å) coordinating

to the θ-$[Mo_8O_{26}]^{4-}$ cluster, so as to avoid the steric hindrance. For compounds **8**−**10**, each M^{II} cation employs one axial oxygen atom coordinating to one two-connected β-$[Mo_8O_{26}]^{4-}$ anion. The octahedral geometry is further completed by three N atoms and two lattice water molecules.

Generally, the M^I cation shows a lower coordination number than the M^{II} cation. For compound **6**, the Cu^I cations take on two-coordinated $[CuN_2]$ and three-coordinated $[CuN_2O]$ styles. We observed the coexistence of two sorts of isomeric forms of β-Mo_8 and γ-Mo_8 in one structure. Such a phenomenon is surprising, although the coexistences of δ-Mo_8 and α-Mo_8 and of α-Mo_8 and β-Mo_8 have been found in the hydrothermal reaction products of $[Cu(bbi)]_2[Cu_2(bbi)_2(\delta\text{-}Mo_8O_{26})_{0.5}][\alpha\text{-}Mo_8O_{26}]_{0.5}$[16] and $[Co(2,2'\text{-bipyridine})_3]_4[Mo_8O_{26}]_2\cdot 5H_2O$,[27] respectively. By replacing L^1 with L^2, we got compound **11** (and **12**, when $M^I = Ag^I$), which holds the same formula as **6** but a different amount of lattice water molecules. However, completely different isomeric forms and framework structures are shown in them. The Cu^I ions exhibit two types of coordination geometries of $[CuN_2]$ and $[CuN_2O_2]$. Each δ-Mo_8 anion in **11** is coordinated with four Cu^I ions through four terminal oxygen atoms from four $[MoO_6]$ octahedra.

Currently, a few compounds containing octamolybdate polyoxoanions and Ag complexes have been reported.[25,28] It seems that the Ag^I ion exhibits subtle interaction with the β-Mo_8 cluster. As illustrated by Cronin et al., Ag^I ions tend to form a $[Ag_2^I]$ dimer, which binds with two distinct square-planar arrangements of four terminal oxygen atoms $[O_4]$ of the β-Mo_8 cluster and links the β-Mo_8 groups forming a whole range of 1D and 2D supramolecular assemblies.[25] Silver−octamolybdate interaction is also included in compound **7**. However, it is the single Ag^I ion that connects the adjacent β-Mo_8 groups into an infinite chain instead of the $[Ag_2^I]$ dimer. By comparing compound **7** with **12**, we found that a minor change of the ligand greatly influences the isomeric forms and the whole framework. As for **7**, we speculate that the coordination of the Ag^I ion with the N−N bridging N atom in the triazole ring of L^1 contributes to such a Ag−β-Mo_8 interaction. It is because the resultant $[Ag_2(L^1)_2]^{2+}$ loop generates greater steric hindrance, which prevents coordination with the Mo_8 anion. As for **12**, due to the coordination of $[AgL^2]$ polymers with the Mo_8 anion, a relatively lower-energy and more-stable δ-type isomer is formed.[11a]

In a word, these results indicate that, during the self-assembly and crystallization process, the change of metal ions and ligands can result in the formation of different peripheral cluster environments which promote the kinetic preference of one isomeric form over another or both. Furthermore, the hydrothermal reaction conditions also provide ample energy for fluxional interconversion between octamolybdate isomers.

(27) Sun, C. Y.; Wang, E. B.; Xiao, D. R.; An, H. Y.; Xu, L. *J. Mol. Struct.* **2005**, *741*, 149.

(28) (a) Abbas, H.; Pickering, A. L.; Long, D. L.; Kögerler, P.; Cronin, L. *Chem.−Eur. J.* **2005**, *11*, 1071. (b) Shi, Z. Y.; Gu, X. J.; Peng, J.; Xin, Z. F. *Eur. J. Inorg. Chem.* **2005**, 3811.

IR Spectra and TG/DTA and PXRD Analyses. The characteristic IR bands of $[Mo_3O_{10}]^{2-}$ and four types (θ, β, γ, and δ) of $[Mo_8O_{26}]^{4-}$ clusters in compounds **1**−**12** are shown in Figure S9 (Supporting Information). The bands at 1625−1108 cm^{-1} are characteristic peaks for the L^1 or L^2 molecules, and the bands at 1092−463 cm^{-1} are ascribed to the υ(Mo=O) and υ(Mo−O−Mo) vibrations. The IR spectra of compounds **1**−**4** (see Figure S9a, Supporting Information) exhibit similar absorption peaks at 1014−583 cm^{-1}, which represent the characteristic peaks of the $[Mo_3O_{10}]^{2-}$ anion. The IR spectra of compounds **8**−**10** (see Figure S9b, Supporting Information) exhibit similar absorption peaks at 1022−463 cm^{-1}, which represent the characteristic peaks of the [β-$Mo_8O_{26}]^{4-}$ anion. Furthermore, the IR spectra of compounds **5**−**7** and **11** and **12** (see Figure S9c, Supporting Information) show big differences of absorption peak positions among the four types of $[Mo_8O_{26}]^{4-}$ anions.

Figure S10 (Supporting Information) displays the calculated and experimental PXRD patterns of compounds **2**−**12**. The diffraction peaks of all calculated and experimental patterns match well. To investigate their thermal stabilities, thermal gravimetric analyses were performed for compounds **2**, **5**−**7**, **10**, and **12** (as shown in Figures S11−S16, Supporting Information). The TG curve shows that **2** loses the coordinated water molecules from room temperature to 277 °C, with an observed mass loss of 4.42%, which is consistent with the theoretical value of 4.57%. The remaining polymeric structure was broken down above 277 °C, and decomposition does not end until heating to 650 °C. For **5**, the TG data show an initial loss of 0.5% (calcd: 0.78%) from room temperature to 150 °C, representing a loss of the crystalline water molecule. The residue remains intact until it is heated to 294 °C, and then mass loss occurs in a consecutive step and does not stop until heating to 1000 °C. The TG curve shows that **6** loses one lattice water molecule (exptl, 0.81%; calcd, 0.74%) per formula unit from room temperature to 120 °C. The residue begins to decompose above 256 °C and does not end until heating to 850 °C. For **7**, the mass loss starts at 284 °C and finishes at ca. 656 °C, which is attributed to the release of two L^1 molecules per formula unit (exptl, 22.60%; calcd, 22.93%). For **10**, there are three distinct weight loss procedures in the range of 45−250 °C, corresponding to the loss of two lattice water and four coordinated water molecules per formula unit (exptl, 4.84%; calcd, 5.07%). The remaining structure was broken down above 280 °C, and decomposition does not end until heating to 800 °C. The TG data show that compound **12** is thermally stable up to around 250 °C, and mass losses occur in a consecutive step and do not stop until heating to 900 °C.

Luminescent Properties. The luminescent properties of free ligands L^1 and L^2 and their polymeric compounds **3**, **6**−**8**, **11**, and **12** were investigated in the solid state. At room temperature, the free L^1 and L^2 show intense absorption at λ_{max} = 262 and λ_{max} = 258 nm in EtOH solutions (see Figures S17 and S18, Supporting Information), respectively. Strong emissions at 289 nm for L^1 and 289, 385, and 419 nm for L^2 are observed. Upon excitation at 262 nm, compounds **3** and **6**−**8** based on L^1 exhibit violet-fluorescent bands at 388 and 419 nm for **3**, 389 and 417 nm for **6**, 390 and 418 nm for **7**, and 385 and 418 nm

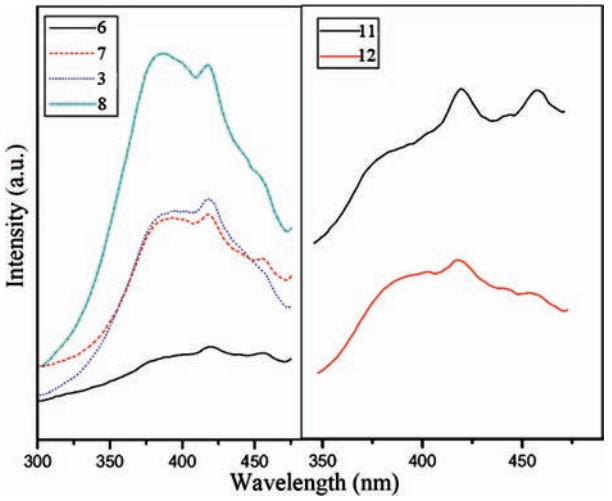

Figure 8. Emission spectra of compounds **3**, **6**−**8** (left), **11**, and **12** (right).

for **8** under the same conditions (Figure 8). As for the compounds based on L^2, the emission spectrum of **11** shows two emission maxima at 419 and 457 nm, while the emission spectrum of **12** exhibits an emission maximum at 418 nm and a broad emission band centered at 458 nm when excitation occurs at 258 nm (Figure 8). As shown in Figure 8, compounds **3** and **6**−**8** based on L^1 have similar luminescent spectra, and compounds **11** and **12** based on L^2 also have similar luminescent spectra, indicating that charge transfer from the free ligand has an obvious effect on the luminescent properties of these compounds. In comparison with the free ligands L^1 and L^2, the emission spectra of compounds **3**, **6**−**8**, **11**, and **12** change largely, and the emission maxima exhibit large red shifts. This may be caused by a change in the highest occupied molecular orbital and lowest unoccupied molecular orbital energy levels of polyoxometalate anions and neutral ligands coordinating to metal centers, and a joint contribution of the intraligand transitions or charge-transfer transitions between the coordinated ligands and the metal centers.[16,20,29]

Conclusion

In summary, a series of novel isopolyoxomolybdate-based frameworks based on $[Mo_3O_{10}]^{2-}$ and four types of $[Mo_8O_{26}]^{4-}$ have been isolated by introducing two flexible ligands into the molybdate system. It is found that the change of metal ions or ligands can result in the formation of different peripheral cluster environments which induce the generation of different $[Mo_8O_{26}]^{4-}$ isomeric forms. This work provides very useful information for assembling isopolyoxoanions and transition metal complexes, and it also demonstrates that the flexible L^1 and L^2 molecules are promising in the assembly process.

Acknowledgment. B-.x. Dong thanks the JSPS for a fellowship.

Supporting Information Available: X-ray crystallographic files for complexes **1**−**12** in CIF format. PXRD patterns and IR spectra of **1**−**12**; emission spectra of L^1 and L^2; TG/DTA curves of compounds **2**, **5**−**7**, **10**, and **12**; selected bond lengths of **1**−**12**; and illustrations of the structures in PDF format. This material is available free of charge via the Internet at http://pubs.acs.org.

(29) (a) Wei, K. J.; Xie, Y. S.; Ni, J.; Zhang, M.; Liu, Q. L. *Cryst. Growth Des.* **2006**, *6*, 1341. (b) Chen, L. J.; He, X.; Xia, C. K.; Zhang, Q. Z.; Chen, J. T.; Yang, W. B.; Lu, C. Z. *Cryst. Growth Des.* **2006**, *6*, 2076.